Greedy Principal Flows

National University of Singapore

Sebastian Lie

05 March 2021

Acknowledgements

First and foremost I would like to thank my supervisor, Prof Yao Zhigang for his invaluable guidance and insight throughout this project. This report and my results would not be the way it is if not for him. To my friends from both Science and Computing: thank you for your companionship, the jokes that keep me amused, and help in the modules we have taken together. You make my days that much brighter. To my friends from CAPT: thank you for the wonderful, thought-provoking conversations, the laughter and the warmth you all bring to my life. Staying in CAPT has been one of the best decisions I have ever made. To my friends from CJC: thank you all for making me laugh so hard and for being a source of comfort. I always look forward to our meet-ups and I always laugh so effortlessly around you all. To Marcus: for being a loveable idiot that has kept me sane through my years schooling. Thank you for being the brother I never had. To my parents: thank you for your unwavering support, advice, love and food. These have been my fuel for the last few months. To Gek: thank you for being a constant who brings much light, warmth and happiness to my life. You are the lighthouse that guides me to shore amongst the stormy seas. Last but definitely not least, I dedicate this to God, the Rock in whom I trust. Through Him all things are possible.

Abstract

Principal Flows are a great tool to use when we want to extend the notion of Principal Component Analysis to multivariate high dimensional data that lie on non-linear lower dimensional manifolds. This is especially since principal flows are curves on a manifold that move along a path of maximal variation of the data, and capture patterns of variation that would escape Principal Component Analysis. Principal flows were originally obtained by solving a problem in variational calculus using the Euler-Lagrange method. In this thesis, we explore the use of a novel, simpler approach to constructing principal flows: a greedy approach. Furthermore, since after rotation, centering, translation and normalisation, vectors can be viewed as points on the hypersphere, we restrict this problem to constructing principal flows on hypersphere. Let us call this new approach the greedy principal flow. We test the effectiveness of our greedy principal flow on toy data, and explore the patterns of variation it finds in real world data. Our results show that our greedy principal flow retains the same effectiveness as the original, and finds meaningful patterns in existing real world data.

Contents

List of Figures

Chapter 1

Introduction

1.1 Motivation

With the advent of Big Data, and massive improvements in computing, machine learning has been used successfully to solve a variety of problems, such as regression and classification problems. However, machine learning can also be used in a more subtle, but no less important way: to discover patterns in the data and glean more information from it. Among methods that have this aim, Principal Component Analysis (PCA) is the most popular and commonly taught. It does however, have a glaring weakness: it does not perform well when the data we are working with is sampled from a non-linear manifold.

This, however is remedied with the principal flow algorithm: it constructs a curve that at each local point moves in the direction of maximal variation and retains canonical PCA interpretation in Euclidean space. Yet, this method is not easy to obtain: we have to solve a problem in variational calculus. What if we could construct this curve with a greedy approach? Could the curve constructed still function as a principal flow? How would it perform on real world data and what new patterns of variation could it yield? These are some of the questions that motivated this thesis.

Chapter one outlines notations and some technical definitions. Chapter two is a literature

review of popular methods in dimension reduction that also help to find patterns in our multivariate data. Chapter three is where we explain how the greedy principal flow is constructed and chapter four is where we present and analyse our results after applying the greedy principal flow on toy and real world data. In the chapter five, we propose future directions of research.

1.2 Notation

Notation	Explanation
$\mathbb{R}^D$	D dimensional Euclidean space.
$\mathbf{X}$	Data matrix of dimensions $n \times D$
$\mathbf{X}_c$	Centered Data matrix of dimensions $n \times D$
D	Dimension of the high-dimensional data.
d	Dimension of the manifold embedded in D dimensional space
$\mathcal{M}^d$	A connected and complete d-dimensional manifold embedded in $\mathbb{R}^D$
p	A point on the manifold, $\mathcal{M}^d$.
$\{p_1, ...p_n\}$	A set of n points on the manifold, $\mathcal{M}^d$.
$\mathbf{v}$	A vector.
$T_p\mathcal{M}$	The Tangent space of a point p on $\mathcal{M}^d$.
$\mathbf{C}$	A Covariance matrix.
$\mathbf{C}_h(p)$	A local tangent covariance matrix with scale h of data on $T_p\mathcal{M}$.
$\{x_1, ...x_n\}$	A collection of n data points in D dimensions. They are also the rows of $\mathbf{X}$
$\mathbf{1}$	A vector of 1s.
$\mathbf{I}$	The identity matrix.
$\mathbf{X}^T$	Transpose of $\mathbf{X}$.
$\mathbf{X}_{(d)}$	d dimensional representation of $\mathbf{X}$
$\mathbf{V}$	A matrix of eigenvectors. where eigenvectors are columns and are sorted in descending order of their eigenvalues.
$\mathbf{\Lambda}$	The diagonal matrix of eigenvalues of $\mathbf{C}$, sorted in descending order.
$\mathbf{V}_{(d)}$	d dimensional representation of $\mathbf{X}$
$\mathbf{S}$	Squared dissimilarity matrix of the data in $\mathbf{X}$ of dimension $n \times n$, calculated with Euclidean distance.
$\otimes$	Outer Product
$\|\cdot\|$	L2-Norm

1.3 Definitions

We note that the section on vector fields is taken from [8].

1.3.1 Vector Fields

A vector at point $\mathbf{x}$, $\mathbf{x} \in \mathbb{R}^D$ is a pair $\mathbf{a} = (\mathbf{x}, \mathbf{v}),\ \mathbf{v} \in \mathbb{R}^D$, such that $\mathbf{v}$ is the vector $\mathbf{v}$ translated so that its tail is at $\mathbf{x}$ instead of the origin. All vector operations are defined such that the first item of the pair remains the same, and the second item is the result of the operation. The length and angle between two vectors are the same as normal vectors rooted in the origin.

Definition: A *vector field* $\mathbf{F}$ on $U \subset \mathbb{R}^D$ is a function which assigns to each point of U a vector at that point. Then

$$\mathbf{F}(\mathbf{x}) = (\mathbf{x}, F(\mathbf{x}))$$

for some function $F : U \longrightarrow \mathbb{R}^D$. Vector fields on $\mathbb{R}^D$ are often most easily described by specifying this associated function F. A pictoral example of a vector field, obtained from [8], is below.

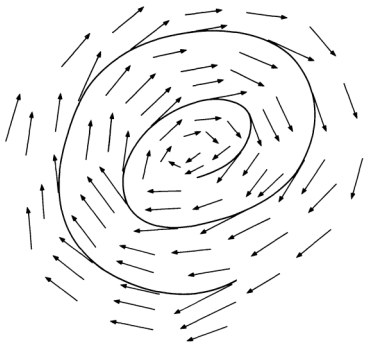

Figure 1.1: An example of a vector field, $\mathbb{R}^3$

A vector field in the context of the diagram is a function that will assign to every point a vector which points in the direction the spiral is moving: from the outer part of the spiral to the inner part.

1.3.2 Geodesics

Geodesics are curves on $\mathcal{M}^d$ which play the same role as straight lines in $\mathbb{R}^d$, Euclidean space. An example of a geodesic on a sphere in $\mathbb{R}^3$ is given by the red curve on the sphere in the figure below, obtained from here [1].

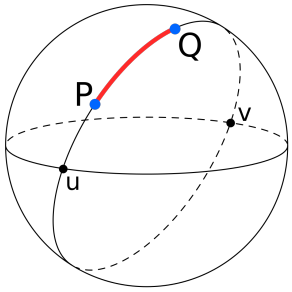

Figure 1.2: Geodesic between P and Q in red on a sphere in $\mathbb{R}^3$

Then, for two points p, q, while our usual Euclidean distance refers to $\|p - q\|$, geodesic distance on the sphere in $\mathbb{R}^3$ is given by the arc length connecting the two points. Intuitively, geodesic distance can be thought of as the "shortest path" between two points on the manifold, $\mathcal{M}^d$.

1.3.3 Exponential Maps

The diagrams below were obtained from [2].

Exponential Map: For each $p \in \mathcal{M}^d$, let

$$exp_p(\mathbf{v}) : T_p\mathcal{M} \longrightarrow \mathcal{M}^d$$

be the exponential map. Let v be a vector $\mathbf{v} = Y - p$ for some $Y \in T_p\mathcal{M}$ we wish to project onto $\mathcal{M}^d$. Then the exponential map moves along the geodesic on $\mathcal{M}^d$ that mirrors the

[1] https://en.wikipedia.org/wiki/Great-circle_distance#/media/File:Illustration_of_great-circle_distance.svg

[2] https://www.researchgate.net/figure/An-exponential-map-exp-X-TX-M-M_fig1_224150233

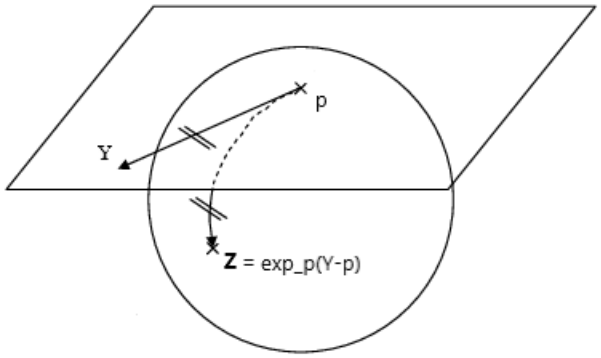

Figure 1.3: Illustration of the exponential map for the three dimensional sphere

direction of $\mathbf{v}$ on $T_p\mathcal{M}$ and finds the projection of Y on $\mathcal{M}^d$.

Logarithm Map: For each $p \in \mathcal{M}^d$, let

$$log_p(z) : \mathcal{M}^d \longrightarrow T_p\mathcal{M}$$

be the logarithm map. It is the inverse of the exponential map: given some point $z \in \mathcal{M}^d$, it finds the vector on $T_p\mathcal{M}$ that mirrors the geodesic going from p to z. This vector indicates the direction in which p should move to obtain the projection of $z \in \mathcal{M}^d$ onto $T_p\mathcal{M}$.

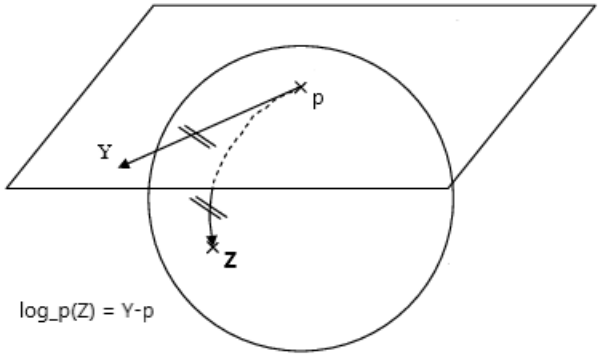

Figure 1.4: Illustration of the log map for the three dimensional sphere

1.3.4 Tangent Space

To define the tangent space we refer to the diagrams below.

Diagrams in figure 1.4 were obtained from here [3] and here [4].

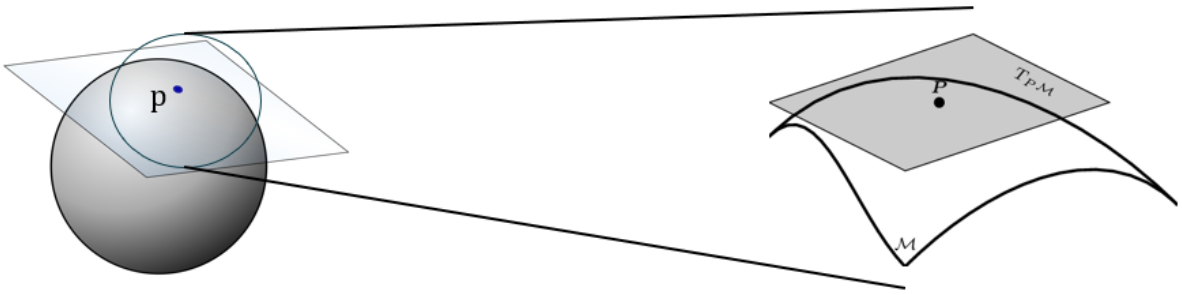

Figure 1.5: Illustration of the tangent space for the three dimensional sphere

Let the three dimensional sphere be the manifold, $\mathcal{M}^d$ and let the blue point be p. Then the plane tangent to $\mathcal{M}^d$ at p is the tangent space, $T_p\mathcal{M}$. Any vectors on this plane lie in $T_p\mathcal{M}$. Then exp_p would project points from the plane down onto the sphere, while log_p would project points from the sphere up to the plane. This is the intuition of the tangent space which we will be working with throughout this thesis. Note that although we specify the manifold and tangent space in three dimensions, we can generalise this to d dimensions, with $\mathcal{M}^d$ as the hypersphere in d dimensions, while $T_p\mathcal{M}$ is the hyperplane. These are the definitions of $\mathcal{M}^d$ and $T_p\mathcal{M}$ we will use when we talk about principal flows later on in chapter three.

[3] https://en.wikipedia.org/wiki/Tangent_space#/media/File:Image_Tangent-plane.svg

[4] https://www.researchgate.net/figure/Conceptual-illustration-of-the-tangent-space-at-point-P-on-a-Riemannian-manifold-M_fig2_262974373

1.3.5 Eigenvalues and Eigenvectors

Let $\mathbf{C} \in \mathbb{R}^{D \times D}$. Then a non-zero vector $\mathbf{v}$ is an eigenvector of $\mathbf{C}$ if there exists some scalar λ such that $\mathbf{C}\mathbf{v} = \lambda\mathbf{v}$. Then λ is known as the eigenvalue corresponding to vector $\mathbf{v}$. Here we also note that for any two eigenvectors v_i and v_j, $i \neq j$, $v_i \cdot v_j = 0$, or any two eigenvectors are orthogonal to each other, and that $v_i \cdot v_i = 1$.

1.3.6 Diagonalisation

We say that a matrix, $\mathbf{C}$, is diagonalisable if there exists an orthonormal matrix such that the rows of that orthonormal matrix are the eigenvectors of $\mathbf{C}$, and a diagonal matrix $\mathbf{\Lambda}$ whose diagonal entries are the eigenvalues of $\mathbf{C}$. In the context of this report, we only consider the eigendiagonalisation of some covariance matrix $\mathbf{C} \in \mathbb{R}^{D \times D}$, which is symmetric and thus, always diagonalisable. Formally, the eigendiagonalisation of $\mathbf{C}$ is given by:

$$\mathbf{C} = \mathbf{V}\mathbf{\Lambda}\mathbf{V}^T$$

From here onwards, we assume there exists a function *diagonalise* that will perform eigendiagonalisation of a matrix and return us all eigenvectors and eigenvalues. We assume further that these eigenvectors and eigenvalues are in sorted order, where the first eigenvector corresponds to the largest eigenvalue.

Chapter 2

Literature Review

2.1 Linear Dimension Reduction

2.1.1 Principal Component Analysis

Principal Component Analysis (PCA) introduced here [3] and expanded in detail here [2] tries to obtain a lower-dimensional representation of the data that retains as much variation as possible present in the data set. PCA relies on constructing principal components (PCs): new variables that are linear combinations of the original variables that have first been centered. These PCs are uncorrelated (orthogonal) and ordered in descending order by the amount of variability of the original data retained. Thus, PCA reduces some high-dimensional data of dimension D to d by computing the first d PCs.

We construct these PCs by first centering the data matrix, $\mathbf{X}$, and obtaining $\mathbf{X}_c$. Next we compute the covariance matrix of the centered data matrix: $\mathbf{C}$. Then we compute the eigendiagonalisation of $\mathbf{C}$, and obtain $\mathbf{V}_d$, a $D \times d$ matrix containing the d eigenvectors associated with the d largest eigenvalues. Here, we note that these d eigenvectors are the d principal directions: directions onto which data is projected to obtain the d PCs. Principal directions will be mentioned again in the later section on Principal Geodesic Analysis and in chapter three. Finally, we get the d PCs by computing $\mathbf{X}\mathbf{V}_d$.

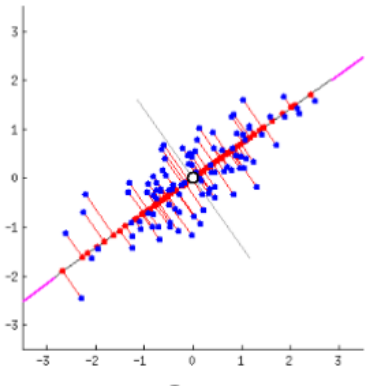

Figure 2.1: PCA in 2 dimensions: data in blue, principal direction as the black line, red points as the first and only PC

The PCA algorithm is outlined below. We assume for simplicity that the following functions are available: *center* that centers a given matrix and *covariance* that computes the covariance of a given matrix.

Algorithm 1: PCA($\mathbf{X}$, d)

Result: $\mathbf{X}_{(d)}$, the d dimensional representation of $\mathbf{X}$, which are the d PCs
$\mathbf{X}_c = center(\mathbf{X})$;
$\mathbf{C} = covariance(\mathbf{X}_c)$;
$\{v_1, ...v_D\}, \{\lambda_1, ...\lambda_D\} = diagonalise(\mathbf{C})$;
$\mathbf{V}_d = \{v_1, ...v_d\}$;
$\mathbf{X}_{(d)} = \mathbf{X}\mathbf{V}_d$;
return $\mathbf{X}_{(d)}$

2.1.2 Classical MDS, Euclidean Distance

Multidimensional Scaling (MDS)'s main aim is find some d dimensional representation of the original data, $\mathbf{X}_{(d)}$, that minimises the discrepancy between the pairwise distances of $\mathbf{X}$ and $\mathbf{X}_{(d)}$, given the squared matrix of pairwise distances of $\mathbf{X}$, $\mathbf{S}$.

Since dissimilarities do not change under translations, we can assume that $\mathbf{X}$ has column means equal to 0. Let $\mathbf{B} = \mathbf{X}\mathbf{X}^T$ be the gram matrix. Let $\mathbf{J}$ be the centering matrix: $\mathbf{J} = \mathbf{I} - n^{-1}\mathbf{1}\mathbf{1}^T$, where $\mathbf{I} \in \mathbb{R}^{n \times n}$ and $\mathbf{1} \in \mathbb{R}^{n \times 1}$ Then, we run MDS by first computing $\mathbf{B} = -\frac{1}{2}\mathbf{J}\mathbf{S}\mathbf{J}$. Next we compute the eigendiagonalisation of $\mathbf{B}$: $\mathbf{B} = \mathbf{V}\mathbf{\Lambda}\mathbf{V}^T$. From the

original $\mathbf{V}$ we take the first d columns: $\mathbf{V}_d$ and the first $d \times d$ submatrix of $\mathbf{\Lambda}$: $\mathbf{\Lambda}_d^{1/2}$. Finally, we compute $\mathbf{X}_{(d)} = \mathbf{V}_d \mathbf{\Lambda}_d^{1/2}$ to obtain the d-dimensional representation of the original data, $\mathbf{X}$. The MDS algorithm is outlined below. Assume we have a function *diagonalise* which computes the first d columns of $\mathbf{V}$ and the $d \times d$ submatrix of $\mathbf{\Lambda}$.

Note that using Euclidean distances, the result of MDS is the same as PCA. The algorithm

Algorithm 2: MDS($\mathbf{S}$, d)

Result: $\mathbf{X}_{(d)}$, the d dimensional representation of $\mathbf{X}$
$\mathbf{J} = \mathbf{I} - n^{-1}\mathbf{1}\mathbf{1}^T$;
$\mathbf{B} = -\frac{1}{2}\mathbf{JSJ}$;
$\{v_1, ...v_D\}, \{\lambda_1, ...\lambda_D\} = diagonalise(\mathbf{B})$;
$\mathbf{V}_d, \mathbf{\Lambda}_d = \{v_1, ...v_d\}, \{\lambda_1, ...\lambda_d\}$;
$\mathbf{X}_{(d)} = \mathbf{V}_d \mathbf{\Lambda}_d^{1/2}$;
return $\mathbf{X}_{(d)}$

and details above are taken from [1] and for a more detailed treatment of MDS we refer there as well. The plot below, obtained from [1] showcases the results of applying MDS to digits, and visualising the results in two dimensions.

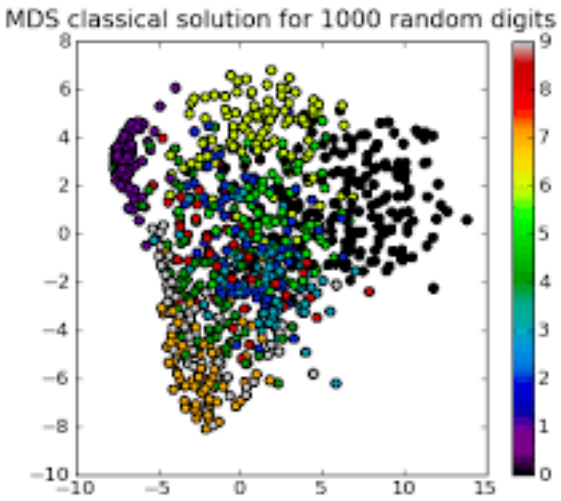

Figure 2.2: Results from Multidimensional Scaling

[1] http://statweb.stanford.edu/~jtaylo/courses/stats306B/mds.html

2.2 Non-Linear Dimension Reduction

Non-linear dimensionality reduction methods are particularly useful when the multivariate data we obtain is sampled from a smooth non-linear manifold $\mathcal{M}^d$, e.g a manifold in an S-shape or a hypersphere. This class of methods obtain better estimates than linear methods like PCA and MDS, especially for the data mentioned above. They are especially successful as certain data sets contain essential non-linear structures that are invisible to PCA and MDS.

2.2.1 Isomap

Isomap, introduced by Tenenbaum et al. [5] is an extension of MDS to manifolds in which embeddings are optimized to preserve geodesic distances between pairs of data points. Isomap achieves this by estimating the geodesic distance between data points, given only input-space distances, e.g Euclidean distance between points.

This relies on the fact that for neighboring points, input-space distance provides a good approximation to geodesic distance. For faraway points, Isomap approximates geodesic distance by adding up a sequence of "short hops" between neighboring points, computed efficiently by finding shortest paths in a graph with edges connecting neighboring data points.

Tenenbaum et al. [5] show this by proving that for a sufficiently high density of data points, we can always choose a neighborhood size large enough that the graph will (with high probability) have a path not much longer than the true geodesic, but small enough to prevent edges that "short circuit" the true geometry of the manifold. This is illustrated in the diagram below, obtained from [5].

Like MDS, Isomap takes as input **S**: a matrix of dissimilarities but differs by first construct-

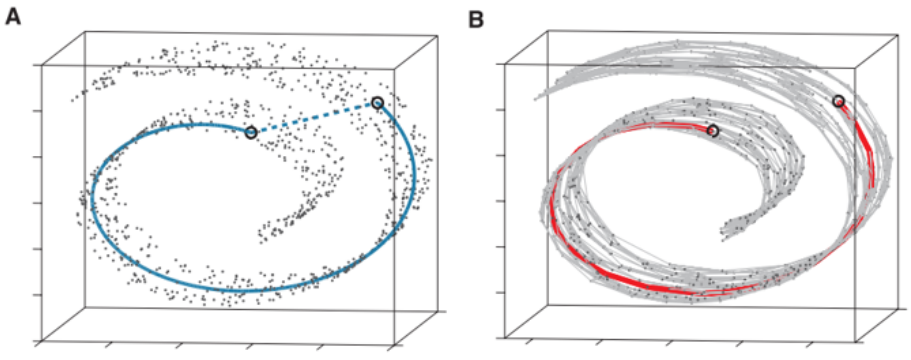

Figure 2.3: Isomap: A the dotted-line distance "short circuits" the manifold , The solid red path in B does not.

ing the neighbourhood graph, G. We start by creating nodes for every data point i. Given some user input K, for every point i, Isomap adds an edge between the i and another point j with weight $S_{i,j}$ if j is one of i's K nearest neighbours. We then run an all pairs shortest

path algorithm on G (we use FloydWarshall here), and obtain a new matrix $\mathbf{A}$, where $\mathbf{A}_{i,j}$ is the shortest distance from i to j. This approximates geodesic distance between i and j. Then we run $MDS(\mathbf{A}, d)$ to obtain $\mathbf{X}_{(d)}$.

The algorithm is outlined below. For simplicity, assume we have a function $ConstructGraph$ which constructs the graph G as explained above.

Algorithm 3: Isomap($\mathbf{S}$, d, K)

Result: $\mathbf{X}_{(d)}$, the d dimensional representation of $\mathbf{X}$
$G = ConstructGraph(\mathbf{S}, K)$;
$\mathbf{A} = FloydWarshall(G)$;
return *MDS(*$\mathbf{A}$*, d)*

2.2.2 Locally Linear Embeddding

Locally Linear Embedding (LLE) introduced by Saul and Roweis [9] aims to construct a mapping from the D dimensional original points to the d dimensional reconstructed points that preserves the local configurations of each point's nearest neighbors. Locally, LLE assumes the embedding is linear, and for each data point $p \in \mathbb{R}^D$, LLE uses a linear combination of its K nearest neighbours to reconstruct a lower-dimensional $p_d \in \mathbb{R}^d$.

Let the set of the i-th point's k nearest neighbours be N_k^i. LLE starts by learning some weights from the D-dimensional data: $\mathbf{W}$ by minimizing the **Reconstruction Error** below using constrained linear fits.

$$\mathbf{RE}(\mathbf{W}) = \sum_{i}^{n} |\mathbf{X}_i - \sum_{j \in N_k^i}^{K} \mathbf{W}_{ij}\mathbf{X}_j|^2$$

Here, $\mathbf{W}$ are the weights that best reconstruct each data point from it's K neighbours, and $\mathbf{W}_{ij}$ represents the contribution of the j-th data point in reconstructing the i-th one. These weights obey an important symmetry: for any particular data point, they are invariant to rotations, rescalings, and translations of that data point and its neighbors. They thus reflect intrinsic geometric properties of the data that are invariant to such transformations, and therefore, we expect their characterization of local geometry in the original data space to be equally valid for local patches on the manifold. This is what motivates our use of $\mathbf{W}_{ij}$ in reconstructing the embedded manifold coordinates in d dimensions.

Next, compute the vectors $\mathbf{Y}_i$ best reconstructed by the weights $\mathbf{W}_{ij}$ by choosing the d dimensional coordinates of each output that minimise the **Embedding Cost Function**:

$$\mathbf{EC}(\mathbf{Y}) = \sum_{i} |\mathbf{Y}_i - \sum_{j} \mathbf{W}_{ij}\mathbf{Y}_j|^2$$

At the end of LLE, each D-dimensional observation $\mathbf{X}_i$ is mapped to a d dimensional $\mathbf{Y}_i$ representing global internal coordinates on the manifold.

A diagram loosely illustrating the procedure above, obtained from [9], is shown below.

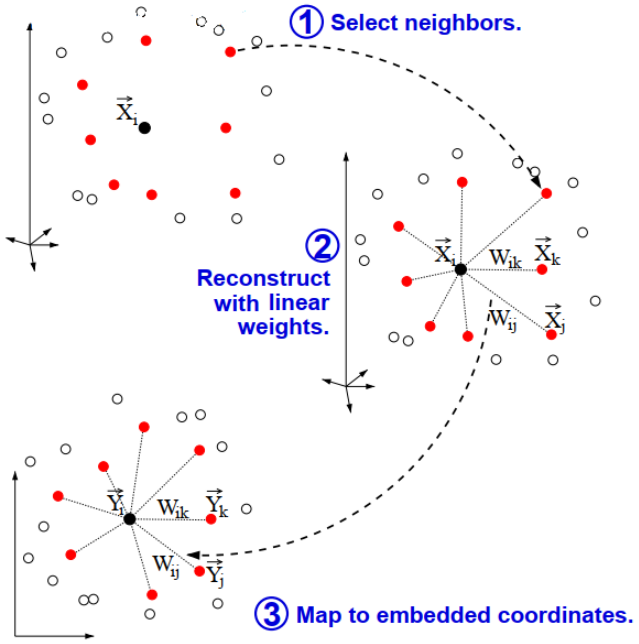

Figure 2.4: Illustration of Locally Linear Embedding Procedure

Algorithm 4: LLE($\mathbf{X}$, d, k)

Result: $\mathbf{X}_{(d)}$, the d dimensional representation of $\mathbf{X}$
First compute N_k^i for all x_i;
$\mathbf{W} = argmin_{\mathbf{W}} \sum_i^n |x_i - \sum_{j \in N_k^i}^k \mathbf{W}_{ij} x_j|^2$;
$\mathbf{X}_{(d)} = argmin_{\mathbf{Y}} \sum_i |\mathbf{Y}_i - \sum_{j \in N_k^i}^k \mathbf{W}_{ij} \mathbf{Y}_j|^2$;
return $\mathbf{X}_{(d)}$

2.2.3 Principal Geodesic Analysis

Principal Geodesic Analysis (PGA) introduced here [4], is a generalization of PCA to manifolds. The main aim of PGA is to describe some D dimensional data that lie on $\mathcal{M}^d$ embedded in $\mathbb{R}^D$. Let $T_p\mathcal{M}$ be the tangent space of $\mathcal{M}^d$ at the intrinsic mean p of the data. The intrinsic mean here is the extension of the concept of the mean in Euclidean space to manifolds. PGA aims to construct some principal geodesics that are analogous to principal

directions in PCA: the directions along which data is projected to obtain a PC.

Instead of finding the principal geodesic however, Fletcher et al. prove that we can approximate the d geodesics along which maximal variation lies by projecting data from $\mathcal{M}^d$ to $T_p\mathcal{M}$ where p is the intrinsic mean of $\{x_1, ..x_n\}$ and then finding the d eigenvectors associated with the d largest eigenvalues of the covariance matrix of the projected data.

PGA begins with computing p by first setting p to a random data point, then iteratively obtaining a better estimate of p. Let p_i be the estimate of p at the i-th iteration. At the i-th iteration, we compute the average of the vectors obtained using the $log_{p_{i-1}}(x_i), \forall x_i$ then set p_i as the projection of that average using $exp_{p_{i-1}}$.

After obtaining p, we calculate the vectors $u_i = log_p(x_i),\ \forall x_i$. Next we calculate the covariance matrix $\mathbf{C} = \frac{1}{n}\sum_{i=1}^{n} u_i u_i^T$. Finally we diagonalise $\mathbf{C}$ to obtain $\{v_k, \lambda_k\}$ the eigenvectors and eigenvalues respectively, which represent the principal directions in the tangent space $T_p\mathcal{M}$ and the variances.

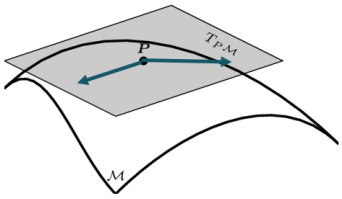

Figure 2.5: An illustration of PGA directions in tangent space approximating principal geodesics

The algorithm for PGA is outlined below.

Algorithm 5: PGA($\{x_1, ...x_n\}$)

Result: $\{v_1, ...v_D\} \in T_p\mathcal{M}$, principal directions and
Variances $\{\lambda_1, ...\lambda_D\} \in \mathbb{R}$
$p =$ intrinsic mean of data $\{x_1, ...x_n\}$;
$u_i = log_p(x_i)$;
$\mathbf{C} = \frac{1}{N}\sum_{i=1}^{N} u_i u_i^T$;
$\{v_1, ...v_D\}, \{\lambda_1, ...\lambda_D\} = diagonalise(\mathbf{C})$;
return $\{v_1, ...v_D\}, \{\lambda_1, ...\lambda_D\}$

Chapter 3

Greedy Principal Flows

3.1 Goal Of Research

The main objective for greedy principal flows is to quantify or describe multivariate data on the manifold: we cannot simply fit a line, as this is not Euclidean space. Instead, we want some curve or path such that, locally, it follows the path of maximal variation of the data in some neighbourhood, but globally also provides the path of maximal "cumulative" variation of the data. These motivate our definition of the principal flow: it is a curve or path on the manifold passing through the mean of the data that is always tangent to the direction of maximal variation of the data at any given point it contains. This path flows outward from the center of the principal flow, the centroid of the data as in the diagram below. The vectors tangent to every point of the principal flow forms a vector field, illustrated by the arrows on the red curve, and each points in the direction of maximum variance. The problem of constructing principal flows has already been solved in [7], where they were constructed by solving a problem in variational calculus.

Therefore, we focus instead on constructing the principal flow using a novel, simpler to implement approach: a greedy algorithm. Here we note that we focus on the first order principal flow, which can be thought of as the manifold extension of the first principal

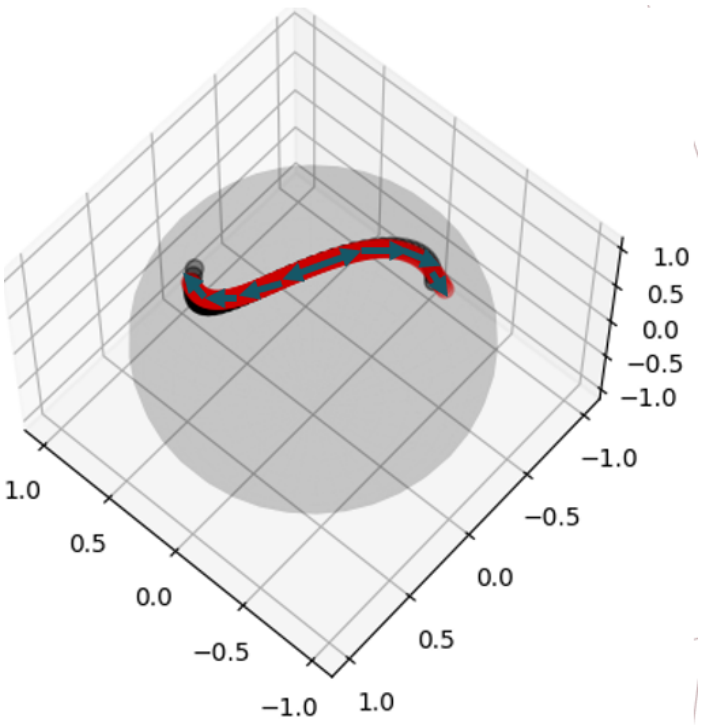

Figure 3.1: The principal flow as a vector field, with the flow in red.

direction in Euclidean space. Additionally, we simplify our approach further and assume that our data $\mathbf{X}$ is some D dimensional data lying on a hypersphere $\mathcal{M}^d$. Thus, our goal is to implement this greedy, simpler version of the principal flow algorithm, and experiment with the results that this implementation of the principal flow algorithm brings. How would it describe various, popular multivariate datasets? Could it find novel ways of describing popular, existing high-dimensional data?

3.2 Centroid Algorithm

Before we get into our principal flow algorithm, we first need to establish our starting point. Since our principal flow follows the path of maximal variation of our data, we know it should pass through the centroid of the data. However, since the data lies on a manifold, we cannot simply use the Euclidean mean of the data points. We need to find the centroid of the data lying on the manifold. Thus, we first aim to estimate this centroid and use it as a starting

point. Although there are many ways of doing this, including the method to find the intrinsic mean in chapter 2.2.3, we opt to make use of the fact that the first principal direction passes through the centroid of the data. To see why this is so, we start with the idea that the first principal direction is the direction that maximises the variance of the data. This can be shown to be equivalent to minimising the reconstruction error of the points projected on this principal direction, which is minimising the sum of squared residuals $\sum(x_i - \hat{x}_i)^2$ where $\hat{x}_i$ are the projected points and x_i are our data points. Notice that this is minimised by obtaining $\hat{x}_i$ that lie on the ordinary least squares (OLS) regression line. And since we can prove that the mean of the data or the centroid of the data lies on the OLS regression line, the centroid of the data does indeed lie on the first principal direction. Thus, if we iteratively project all the data onto the tangent space of the hypersphere, find the first principal direction, move in that direction, and find the projected point on the hypersphere, we will eventually converge on the centroid. The algorithm to find the centroid is outlined below.

Algorithm 6: Centroid($\{x_1, ...x_n\}$)

Result: p, centroid of the data
p = a random data point from $\{x_1, ...x_n\}$;
for $i = 1 \rightarrow max\_iter$ **do**
  Compute $u_i = log_p(x_i)$ for all x_i,;
  $\mathbf{C} = \frac{1}{N}\sum_{i=1}^{N} u_i u_i^T$;
  v_1 = eigenvector corresponding to the largest eigenvalue of $\mathbf{C}$;
  $p' = p + \epsilon v_1$;
  $p = exp_p(p')$;
return p

3.3 Algorithm

Now we move on to outlining and elaborating on the greedy principal flow algorithm. Let p_i be the point on the principal flow obtained from the i-th iteration where p_0 is the first point on the principal flow: the centroid from the algorithm in the previous section. Before we start our principal flow algorithm we first need to decide on the maximum number of

iterations. This will determine the number of points on each side of the principal flow, not counting the original point: the centroid. Now we explain the procedure of the principal flow at the i-th iteration.

We note that for the i-th iteration, we apply the following procedure to both ends of the principal flow. First, we project $\mathbf{X}$ onto the hyperplane at p_{i-1}, $T_{p_{i-1}}\mathcal{M}$. Here we may choose to project all our data, or use a kernel function, $\mathcal{K}$ to weight our data so that more emphasis is placed on points in some neighborhood around p_{i-1}, whose size is controlled by scale parameter h, than outside it. Intuitively, h controls how sensitive the principal flow is to local data. We define $\{w_i, ...w_n\}$ as the weights from our kernel function. For our algorithm, we implement three choices of kernel functions: the binary kernel which weights points as one or zero depending on their distance from p, the gaussian kernel which weights points according to the gaussian distribution based on their distance from p and lastly the identity kernel, which sets all weights to be one.

Thus, we first apply our kernel function to the data, and obtain weights $\{w_i, ...w_n\}$, then apply our log map $log_{p_{i-1}}$ to project our data on $T_{p_{i-1}}\mathcal{M}$ obtaining a matrix of vectors on $T_{p_{i-1}}\mathcal{M}$ that point from p to the projected points. These $log_{p_{i-1}}(x_i)$ are our plane vectors. Then we compute the covariance matrix of the plane vectors using both our weights and our plane vectors by the equation below obtained from [7].

$$C_h(p) = \frac{1}{\Sigma_i \mathcal{K}_h(x_i, p)} \sum_{i=1}^{n} (log_{p_{i-1}}(x_i) \otimes log_{p_{i-1}}(x_i)) \mathcal{K}_h(x_i, p)$$

We then perform eigendiagonalisation of the covariance matrix and take the eigenvector v_1 corresponding to the largest eigenvalue λ_1. This indicates the direction of the principle flow and is our principal direction. Here, λ_1 corresponds to the amount of variance of our data in the direction of v_1. This is where the "greediness" in our algorithm lies: since we choose at each step, the direction of maximum variance.

If this is the first iteration, then p_{i-1} is the centroid of the data. Thus, we collect two

points: one point when we move a step size of ϵ in the principal direction, and the other when we move a step size of ϵ in the opposite of the principal direction. We then project both points back onto $\mathcal{M}^d$, using $exp_{p_{i-1}}$. Set p_1 to be the first point, and p_opp_1 to be the second. Otherwise, we first check that this principal direction is in the same direction as the previous principal direction of this end of the flow, and if not, apply a negative sign to the principal direction. Then for each end of the flow, we move a step size of ϵ in the principal direction at that end, then project both points back onto $\mathcal{M}^d$, using the exponential map. We repeat the procedure above until the maximum iterations is reached.

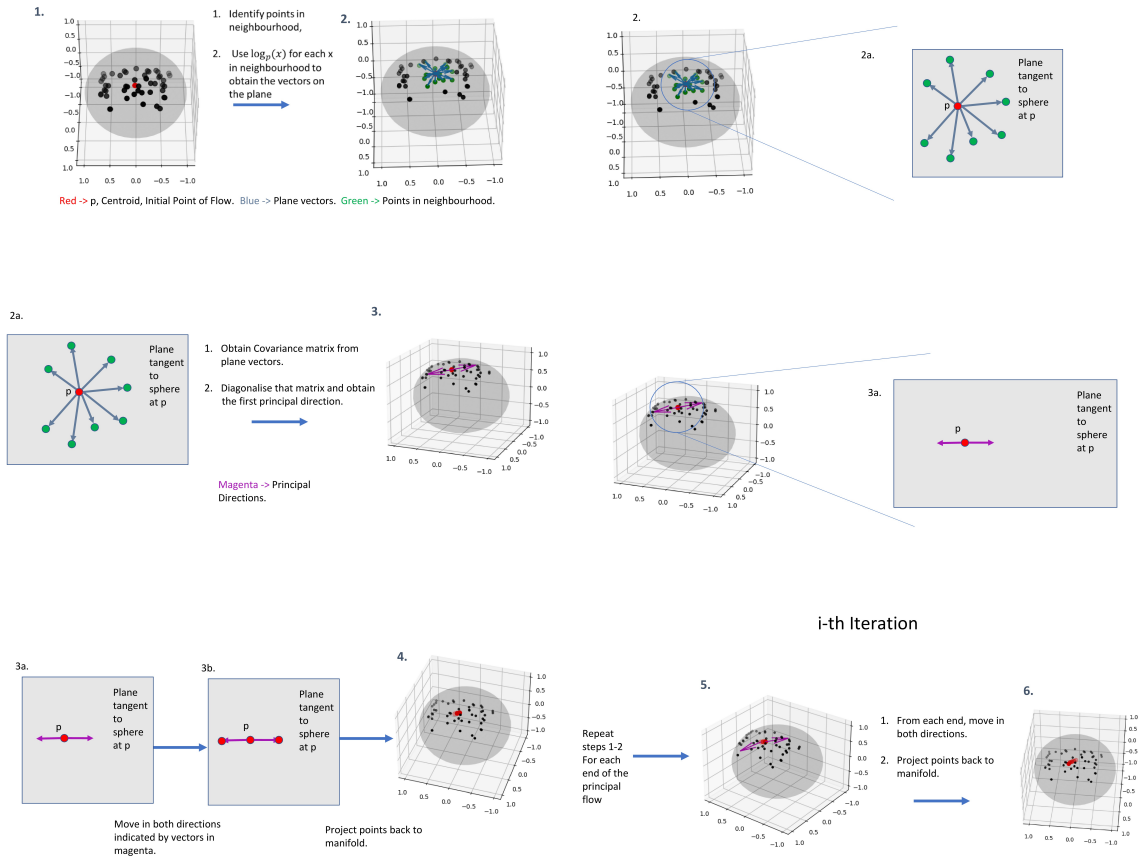

Figure 3.2: Illustration of the Greedy Princpal flow algorithm. The first four steps cover the first iteration, while five and six cover the i-th iterations.

The Greedy Principal Flow algorithm is outlined below.

Algorithm 7: GreedyPrincipalFlow($\{x_1, ...x_n\}$, *centroid*, $\mathcal{K}$, *max_iter*, h, ϵ)

Result: $\{p_0, .., p_m\} \bigcup \{p\_opp_1, .., p\_opp_m\}$, points on the principal flow

$m = max\_iter$;
$p_0 = centroid$;
$p\_opp_0 = centroid$;
for $i = 1 \rightarrow m$ **do**
  if $i == 1$ **then**
    $\{w_i, ...w_n\} = \mathcal{K}(h, p_{i-1}, \{x_1, ..., x_n\})$;
    $\mathbf{C}_h(p_{i-1}) = \frac{1}{\Sigma_i w_i} \sum_{i=1}^{n} (log_{p_{i-1}}(x_i) \otimes log_{p_{i-1}}(x_i)) w_i$;
    $\{v_1, ..., v_n\}, \{\lambda_1, ...\lambda_n\} = diagonalise(\mathbf{C}_h(p_{i-1}))$;
    $principal\_direction = v_1$;
    $principal\_direction\_opp = -v_1$;
  else
    $\{w_i, ...w_n\} = \mathcal{K}(h, p_{i-1}, \{x_1, ..., x_n\})$;
    $\mathbf{C}_h(p_{i-1}) = \frac{1}{\Sigma_i w_i} \sum_{i=1}^{n} (log_{p_{i-1}}(x_i) \otimes log_{p_{i-1}}(x_i)) w_i$;
    $\{v_1, ..., v_n\}, \{\lambda_1, ...\lambda_n\} = diagonalise(\mathbf{C}_h(p_{i-1}))$;
    if $cos^{-1}(v_1^T principal\_direction\_past) > \pi/2$ **then**
      $v_1 = -v_1$;
    $principal\_direction = v_1$;
    $\{w_i, ...w_n\} = \mathcal{K}(h, p\_opp_{i-1}, \{x_1, ..., x_n\})$;
    $\mathbf{C}_h(p\_opp_{i-1}) = \frac{1}{\Sigma_i w_i} \sum_{i=1}^{n} (log_{p\_opp_{i-1}}(x_i) \otimes log_{p\_opp_{i-1}}(x_i)) w_i$;
    $\{v_1, ..., v_n\}, \{\lambda_1, ...\lambda_n\} = diagonalise(\mathbf{C}_h(p\_opp_{i-1}))$;
    if $cos^{-1}(v_1^T principal\_direction\_opp\_past) > \pi/2$ **then**
      $v_1 = -v_1$;
    $principal\_direction\_opp = v_1$;
  $p_i = exp_{p_{i-1}}(p_{i-1} + \epsilon principal\_direction)$;
  $p\_opp_i = exp_{p\_opp_{i-1}}(p\_opp_{i-1} + \epsilon principal\_direction\_opp)$;
  $principal\_direction\_past = principal\_direction$;
  $principal\_direction\_opp\_past = principal\_direction\_opp$;
return $\{p_0, .., p_m\} \bigcup \{p\_opp_1, .., p\_opp_m\}$

3.4 Extension: Greedy Principal Boundary

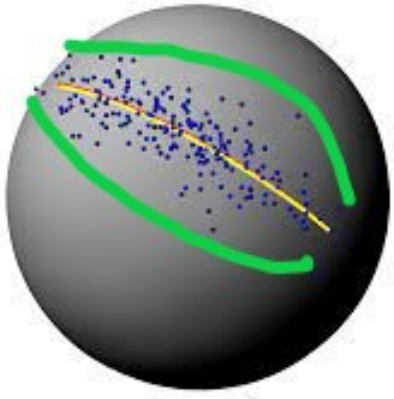

Figure 3.3: Principal Boundary in green around the data in blue for the three dimensional sphere

In the section above, we have already seen the principal flow. Now we extend the idea of principal flows to attempt to find some boundary of the data. Let us assume that the data is contained on some ellipse of the manifold $\mathcal{M}^d$. Then our aim is to find some boundary around this ellipse. We proceed similarly to the principal flow, except that we now save $v_1, v_2, \lambda_1, \lambda_2$ when we diagonalise $\mathbf{C}_h(p_{i-1})$. and use them to compute the boundaries of data.

Let $b_{i,1}$ be the first boundary point of the i-th principal flow point. Then at each iteration, the boundary b is calculated before p is updated by $b_{i,1} = exp_{p_{i-1}}(p_{i-1} + \frac{\lambda_2}{\lambda_1} * radius * v_2)$ and $b_{i,2} = exp_{p_{i-1}}(p_{i-1} - \frac{\lambda_2}{\lambda_1} * radius * v_2)$ where radius is a user specified parameter. Intuitively, we try to move a distance in the direction of v_2 orthogonal to the principal flow that approximates the radius of the ellipse that contains the data, $\mathbf{X}$.

Algorithm 8: GreedyBoundaryFlow($\{x_1, ...x_n\}$, $centroid$, $\mathcal{K}$, max_iter, $h, \epsilon, radius$)

Result: $\{p_0, .., p_m\} \bigcup \{p\_opp_1, .., p\_opp_m\} \bigcup \{b_{0,1}, .., b_{m-1,2}\} \bigcup \{b\_opp_{1,1}, .., b\_opp_{m-1,2}\}$, points and boundary of the principal flow

$m = max\_iter$;
$p_0 = centroid$;
$p\_opp_0 = centroid$;
for $i = 1 \rightarrow m$ **do**
  if $i == 1$ **then**
    $\{w_i, ...w_n\} = \mathcal{K}(h, p_{i-1}, \{x_1, ..., x_n\})$;
    $\mathbf{C}_h(p_{i-1}) = \frac{1}{\Sigma_i w_i} \sum_{i=1}^{n} (log_{p_{i-1}}(x_i) \otimes log_{p_{i-1}}(x_i)) w_i$;
    $\{v_1, ..., v_n\}, \{\lambda_1, ...\lambda_n\} = diagonalise(\mathbf{C}_h(p_{i-1}))$;
    $b_{i-1,1} = exp_{p_{i-1}}(p_{i-1} + \frac{\lambda_2}{\lambda_1} * radius * v_2)$;
    $b_{i-1,2} = exp_{p_{i-1}}(p_{i-1} - \frac{\lambda_2}{\lambda_1} * radius * v_2)$;
    $principal\_direction = v_1$;
    $principal\_direction\_opp = -v_1$;
  else
    $\{w_i, ...w_n\} = \mathcal{K}(h, p_{i-1}, \{x_1, ..., x_n\})$;
    $\mathbf{C}_h(p_{i-1}) = \frac{1}{\Sigma_i w_i} \sum_{i=1}^{n} (log_{p_{i-1}}(x_i) \otimes log_{p_{i-1}}(x_i)) w_i$;
    $\{v_1, ..., v_n\}, \{\lambda_1, ...\lambda_n\} = diagonalise(\mathbf{C}_h(p_{i-1}))$;
    $b_{i-1,1} = exp_{p_{i-1}}(p_{i-1} + \frac{\lambda_2}{\lambda_1} * radius * v_2)$;
    $b_{i-1,2} = exp_{p_{i-1}}(p_{i-1} - \frac{\lambda_2}{\lambda_1} * radius * v_2)$;
    if $cos^{-1}(v_1^T principal\_direction\_past) > \pi/2$ **then**
      $v_1 = -v_1$;
    $principal\_direction = v_1$;
    $\{w_i, ...w_n\} = \mathcal{K}(h, p\_opp_{i-1}, \{x_1, ..., x_n\})$;
    $\mathbf{C}_h(p\_opp_{i-1}) = \frac{1}{\Sigma_i w_i} \sum_{i=1}^{n} (log_{p\_opp_{i-1}}(x_i) \otimes log_{p\_opp_{i-1}}(x_i)) w_i$;
    $\{v_1, ..., v_n\}, \{\lambda_1, ...\lambda_n\} = diagonalise(\mathbf{C}_h(p\_opp_{i-1}))$;
    $b\_opp_{i-1,1} = exp_{p\_opp_{i-1}}(p\_opp_{i-1} + \frac{\lambda_2}{\lambda_1} * radius * v_2)$;
    $b\_opp_{i-1,2} = exp_{p\_opp_{i-1}}(p\_opp_{i-1} - \frac{\lambda_2}{\lambda_1} * radius * v_2)$;
    if $cos^{-1}(v_1^T principal\_direction\_opp\_past) > \pi/2$ **then**
      $v_1 = -v_1$;
    $principal\_direction\_opp = v_1$;
  $p_i = exp_{p_{i-1}}(p_{i-1} + \epsilon principal\_direction)$;
  $p\_opp_i = exp_{p\_opp_{i-1}}(p\_opp_{i-1} + \epsilon principal\_direction\_opp)$;
  $principal\_direction\_past = principal\_direction$;
  $principal\_direction\_opp\_past = principal\_direction\_opp$;
return $\{p_0, .., p_m\} \bigcup \{p\_opp_1, .., p\_opp_m\} \bigcup \{b_{0,1}, .., b_{m-1,2}\} \bigcup \{b\_opp_{1,1}, .., b\_opp_{m-1,2}\}$

Chapter 4

Applications

Writing the algorithm is meaningless without testing that it also functions as we want it to. First we start with simple applications on toy data to confirm that our algorithm works as intended, then we apply it on some real world data to show how the principal flow can be used there as well.

4.1 Toy Data

4.1.1 Without Noise

As a sanity check or proof of concept of our principal flow, we first want to test our algorithm on some toy data that we know lies on the three-dimensional unit sphere. This will help us visualise the flow created and determine if it follows the pattern of the data, and thus act as a proof of concept of our novel approach to principal flows. We first generate some data artificially.

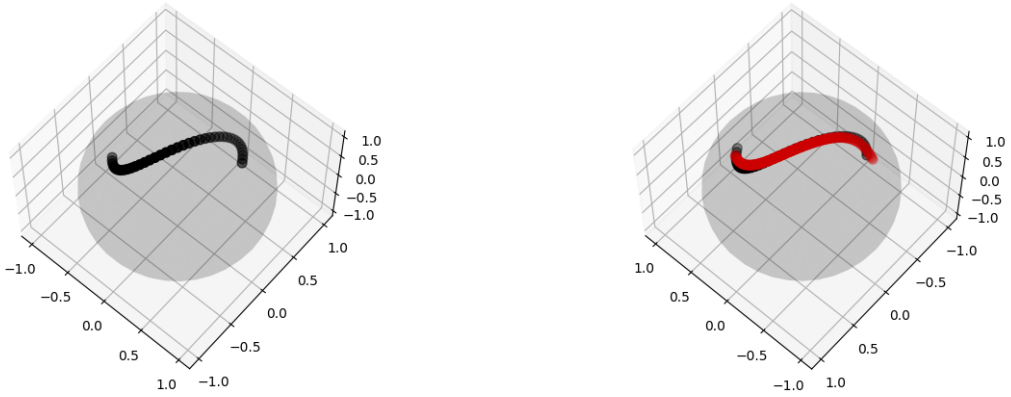

(a) Toy data 13, $\mathbb{R}^3$ (b) Principal Flow on Toy Data, $\mathbb{R}^3$

Figure 4.1: Principal flow, no noise

For example, this dataset is created by setting the first coordinate of the i-th point, $x_{i,1} = \frac{i-n/2}{n}$, then $x_{i,2} = sin(4 * x_{i,1})/2$, and the third to $x_{i,3} = \sqrt{1 - x_{i,1}^2 - x_{i,2}^2}$, where n is the number of points we want to generate.

Now that we have seen the Toy Data, let us apply the Principal Flow algorithm to the data above. This 3D plot shows the original data in black, and the principal flow in red. With some tuning of h, the size of the neighbourhood, we can see that we have constructed a principal flow that follows the original data almost exactly, reconstructing an "S" with some slight differences at the curves of the s-shape of the original data. We have now seen that proof that our principal flow algorithm works: it is able to accurately reconstruct the toy data, the s curve on the sphere.

4.1.2 With Noise

Next, gaussian noise was added to the S-shaped data on the sphere to create a noisy dataset. Then we fitted a principal flow to this noisy data.

We can see that the principal flow obtained seems to follow the new pattern of variation in the data: from the more dense cloud of points on the left, to the curve of the points in the center to the other dense cloud of points on the right. We can see from these examples

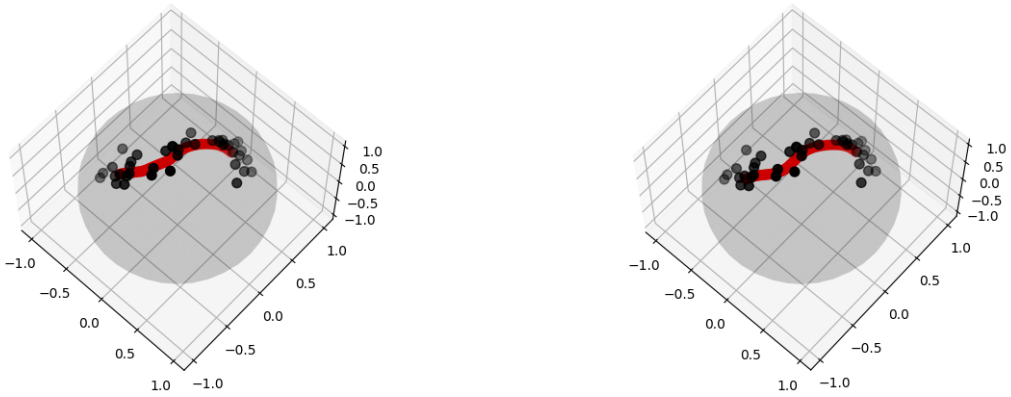

(a) Flow on Noisy Data using binary kernel (b) Flow on Noisy Data using gaussian kernel

Figure 4.2: Principal flow, noisy data, both kernels run with similar h

that even with noise, our algorithm is able to discern the pattern of the data.

4.1.3 Boundary Flow with Noise

Next we test out our extension, our algorithm for our principal boundary.

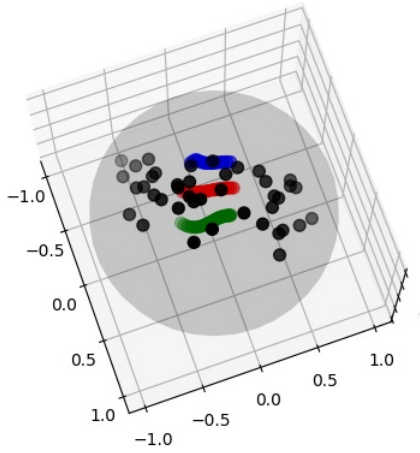

Figure 4.3: Boundary Flow on noisy data

Since we need a "cloud" of data, we apply some gaussian noise on the data from above, and then run our principal boundary algorithm on it. Let the principal flow be the curve in red,

and the boundaries be in blue and green.

With some tuning, we obtain these three curves: we can see that the principal flow is in the middle of the dataset, while the boundary flows accompany it in parallel and even form to the shape of the cloud of data, bending outwards when there is a point beyond it. Through this graph, we can see how the principal boundary can work and be shaped by the shape of the cloud of data.

4.2 Real World Data

Our results on artificial data are promising, however, it means little if there are no real-world applications for our greedy principal flow. In this section we test our results on two real-world datasets: the MNIST dataset and the Olivetti face dataset. Extra results are included in the appendix.

4.2.1 MNIST

We first test the principal flow algorithm on the MNIST dataset, a rite of passage for machine learning algorithms. The MNIST dataset is a set of handwritten digits. We run our principal flow algorithm using the binary kernel on just handwritten 3s alone.

These images in the diagram below, read from left to right, top to bottom, are points from the greedy principal flow using the binary kernel. Although it does not represent all the variability of the 3s in the dataset, we can see that all the images obtained are "nice" representations of 3s, in that they cannot be confused with any other digit, and they seem to be quite neatly written. Our principal flow algorithm obtaining these representations suggests that it has found some path through the data that has intuitive meaning: the images from this path are easily discernable, and seems to validate our choice of a hypersphere for $\mathcal{M}^d$, since data that intuitively should be "near" each other, such as 3s that look the same, are indeed close on $\mathcal{M}^d$. Within these "nice" 3s then we observe the source of the variability: the slant of the digit. We can see that the digits start out leaning right with the upper left group of images, then slowly rotate to slant to the left, going through a phase of being perfectly centered.

This perhaps is an insight into the well-written 3s in the dataset and perhaps of neat handwritten digits in general: that the upper and middle part of the digit differ mainly in orientation, while the tail remains mostly fixed. Additionally, this gradual change in orientation of the digit along the curve suggests that our greedy principal flow is able to find a central

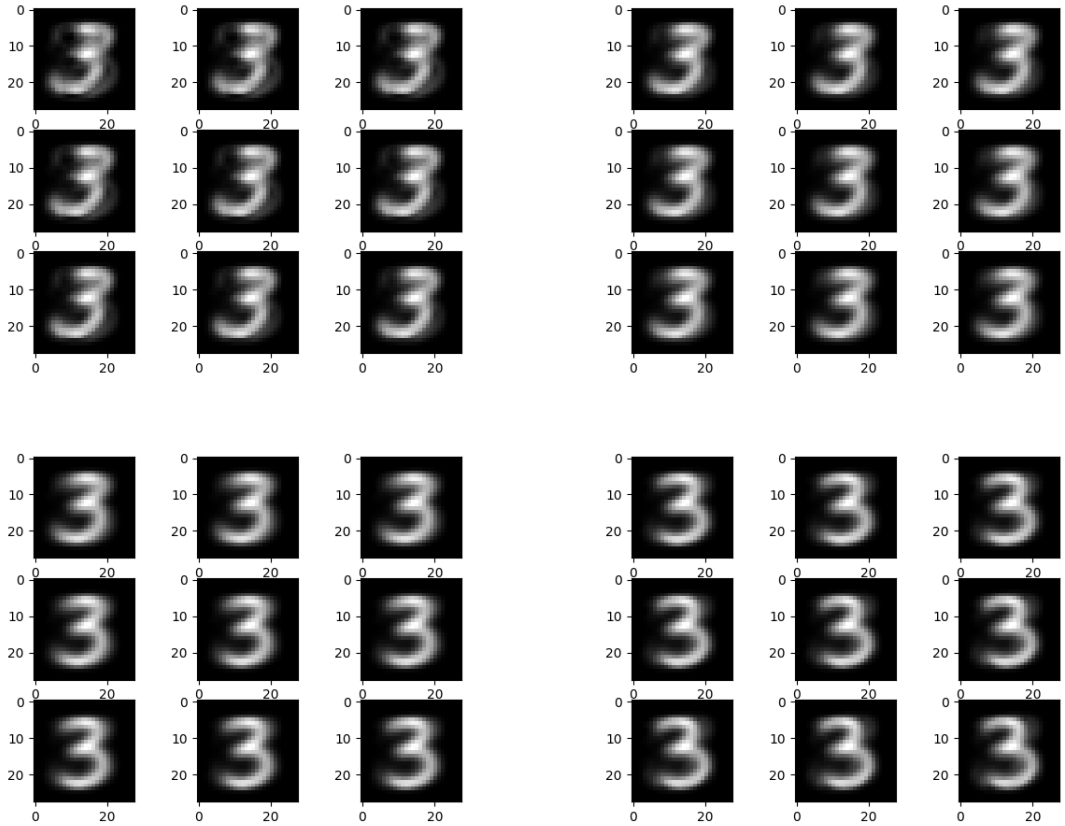

Figure 4.4: MNIST Flows, from left to right.

path that not only describes variability present in the data, but that also translates to some real world meaning. From our results from the MNIST data, we can see that our greedy principal flow can be used to understand our data better, and seek out some patterns of variation that we might otherwise be oblivious too.

4.2.2 Olivetti faces

Next we test our algorithm on a facial dataset. The Olivetti face dataset is a set of 64x64 images taken between April 1992 and April 1994 at AT&T Laboratories Cambridge. Although the main website for the dataset is no longer functioning, it can be obtained from several other websites. Our version was obtained from `sklearn`, a package in python.

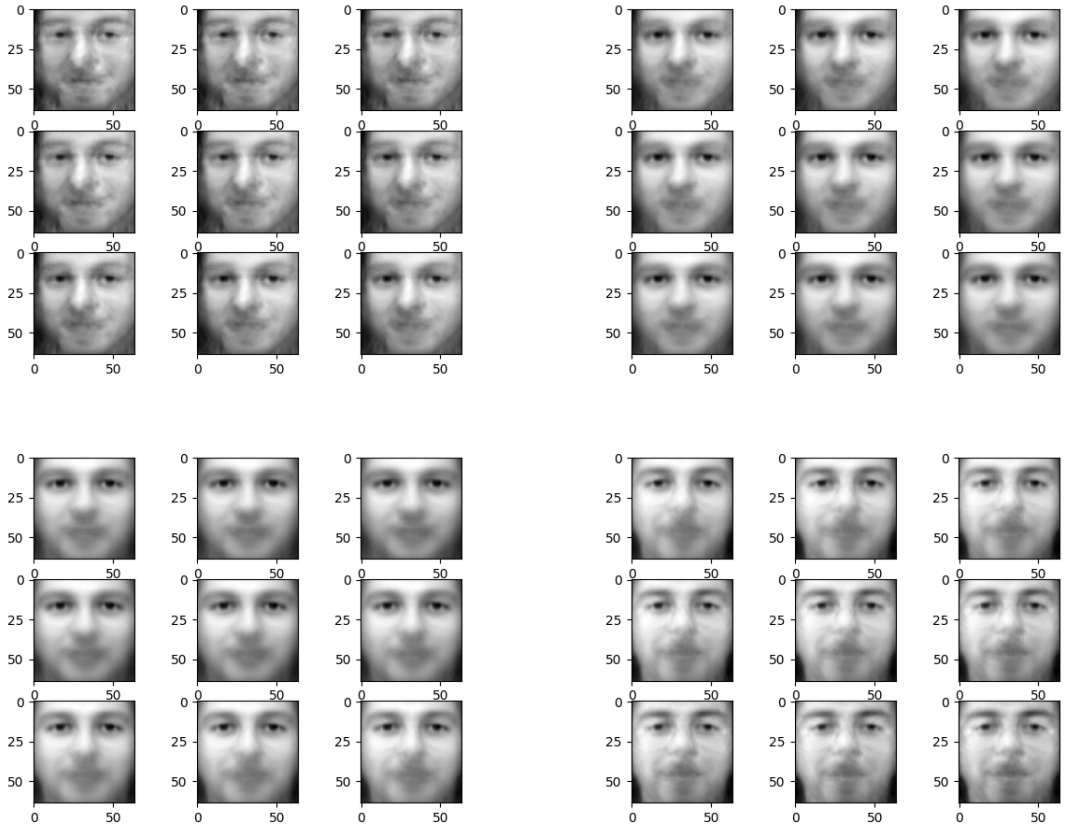

Figure 4.5: Flow for Olivetti face data, from left to right.

We can see that the principal flow obtained contains clear pictures of faces, albeit with the bottom half of their faces slightly blurred. As with our results from the MNIST data, we can glean meaning from neighbouring images on the curve: they are close to each other in a meaningful way. This can be seen from how the set of faces on the upper left and some in the upper right are slightly tilted away from us, but gradually transition to facing us in the

last few images of the upper right set. These smooth transitions tell us that on $\mathcal{M}^d$, a face slightly tilted away is near a face directly facing the camera which makes intuitive, real world sense. This is another indication that our choice of $\mathcal{M}^d$ does yield fruit and preserve some real world interpretation, which validates our approach of restricting $\mathcal{M}^d$ to the hypersphere. Observing the images closely, we can see that these faces differ the most in the angle of their face, whether they wear glasses (first few images on upper left), and whether they have a beard (last two images, bottom right and first three images, upper left). While capturing the difference in the angle of faces in the images that we might not have noticed immediately is good, we observe that the pictures here seem to be that of only men. It seems like our principal flow captures the variability between men more so than between men and women. However, this perhaps makes more intuitive sense: facial images of men without glasses or a beard differ more from a facial image of a man with these features than an image of a woman's face would. Through our results here, we can see that while our greedy principal flow incorporates mostly local information (i.e the faces in some neighbourhood around our current flow point), the flow obtained is also open to a more global interpretation: we can see the faces transition through different angles, tilting in the same direction continuously, and watch as it describes to us the main sources of variation in the data set.

Chapter 5

Future Directions

The topic of principal flows and manifold learning in general is a rich field with much potential, and there are many avenues of expanding the work done in this report. One potential direction is constructing the k-th order principal flows, where $k > 1$. Another potential avenue of research is using different kinds of $\mathcal{M}^d$. In this report, we have restricted ourselves only to the hypersphere. Although this might be a "good enough" approximation, if we had intuition about the specific form of the manifold on which our multivariate data lies, and we determine that the hypersphere is unsuitable, then this current principal flow would not be able to accomodate this intuition. With a different manifold, we might be able to obtain a different principal flow that might give us more information about the variability of the data and describe it more appropriately than using the hypersphere. Additionally, we could also extend the greedy principal boundary to be a maximal margin classifier. Although this has already been done in [6], it has yet to be done with a greedy approach, and would be the first greedy maximal margin classifier for multivariate data lying on some Riemannian manifold.

Bibliography

[1] Borg, I., and Groenen, P. J. F. (2005), *Modern Multidimensional Scaling, Theory and Applications*, 2 edn Springer.

[2] Jollife, I. T. (2002). *Principal Component Analysis*, 2 edn Springer.

[3] Pearson, K. (1901). "On Lines and Planes of Closest Fit to Systems of Points in Space". *Philosophical Magazine*. 2 (11): 559–572.

[4] Fletcher, P. T., Lu, C., Pizer, S. M., and Joshi, S. (2004), "Principal Geodesic Analysis for the Study of Nonlinear Statistics of Shape," *IEEE Transactions on Medical Imaging*, 23, 995-1005.

[5] Tenenbaum, J. B., Silva, V. D., and Langford, J. C. (2000). "A Global Geometric Framework for Nonlinear Dimensionality Reduction," *Science*, 290, 2319-2323.

[6] Yao, Z., and Zhang, Z. (2019) "Principal Boundary on Riemannian Manifolds," *Journal of the American Statistical Association* 115(531), 1435–1448.

[7] Panaretos, V. M., Pham, T., and Yao, Z. (2014), "Principal Flows" *Journal of the American Statistical Association*, 109, 424-436.

[8] Thorpe, J. A. (1979). *Elementary Topics in Differential Geometry*, Springer.

[9] Roweis, S. T., and Saul, L. K. (2003). "Think Globally, Fit Locally: Supervised Learning of Low Dimensional Manifolds." *Journal of Machine Learning Research*, 4, 119–155.

Appendices

Appendix A

Extra Results from the Principal Flow

A.1 Fashion MNIST

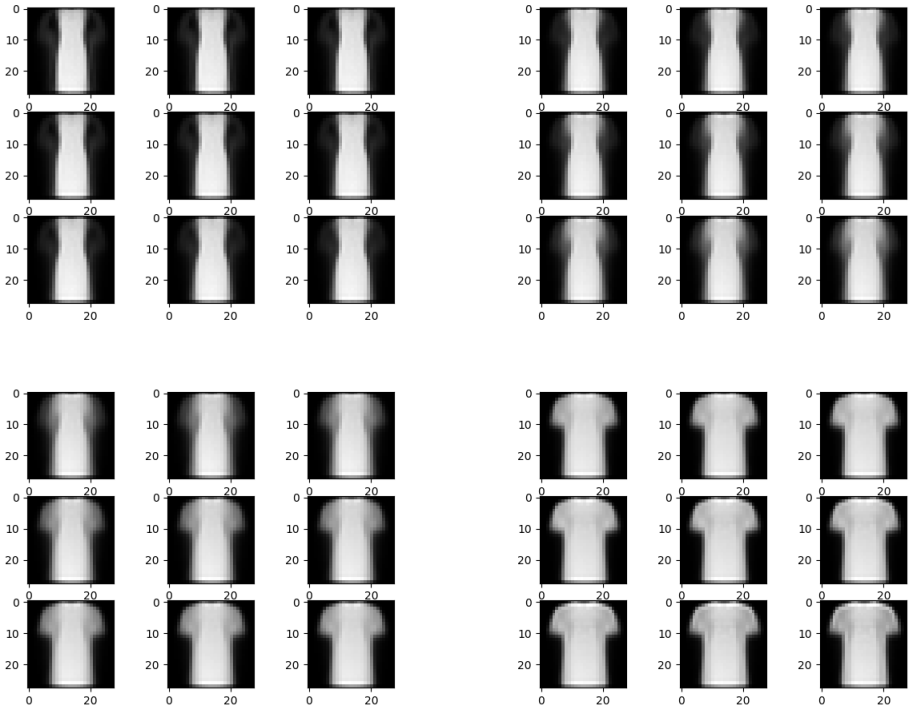

Figure A.1: Fasion MNIST Flows, from left to right.

Here we test our principal flow on objects, and rather on 2 pieces of fashion that look

quite alike: t-shirts and dresses. Here we can watch as dresses morph into t-shirts. More than just an interesting graphic, it shows that the principal flow is able to capture the variability of the data: here the data varies very clearly in the outline of the images, and images on the principal flow reflect this main source of variability.

A.2 Cartoon Faces

Now we test our principal flow on a dataset of cartoon faces.

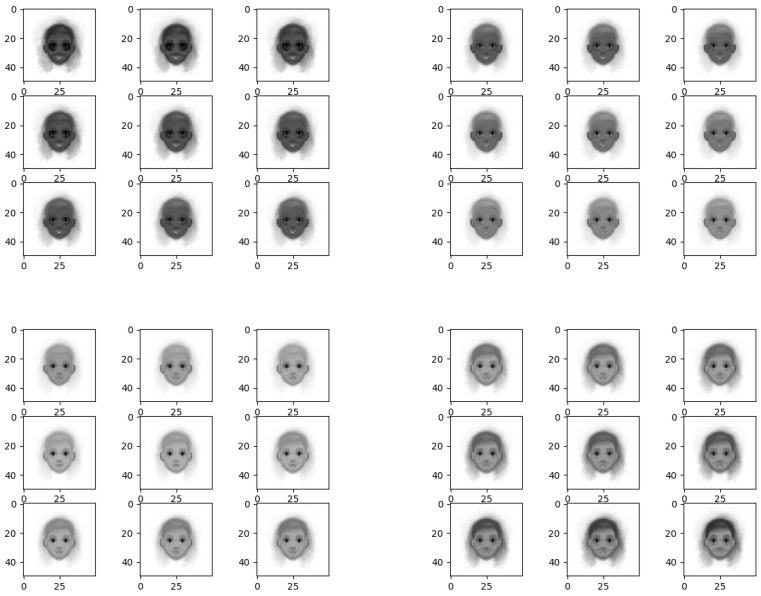

Figure A.2: Cartoon face Flows, from left to right.

When run on a dataset of cartoon faces, the principal flow finds a series of faces that differ greatly in skin color and in hair color. Along the flow we can see that the faces start with a dark skin color and gradually transition to a lighter skin color, then get darker along with their hair color. Here we can see that faces vary mainly on skin tone and hair color, which makes intuitive sense, since other features like spectacles and a particular hair shape may not feature on many data points.

A.3 Faces in the Wild

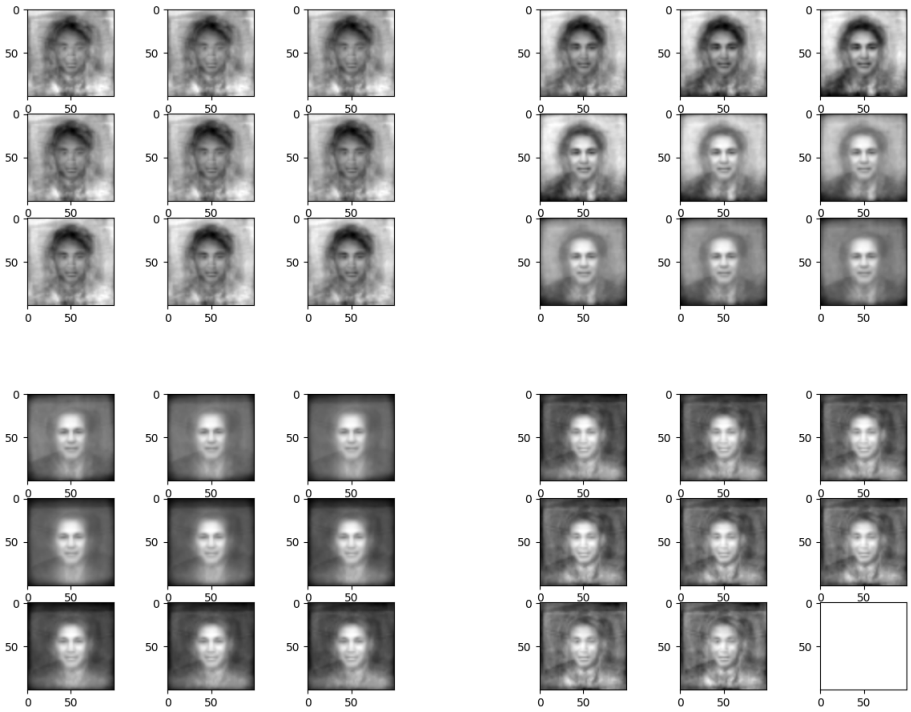

Figure A.3: Faces in the wild flow, from left to right.

Here we test our principal flow algorithm on real faces with differing backgrounds, since these are photos found online. As with the cartoon faces, we can see that these faces differ in skin tone but also in eyebrow color, eye shape and background. This makes sense, since skin tone will determine a large portion of the face, and the background also takes up a large part of the images, and are likely to differ quite greatly.